An electron spin resonance study of thermoluminescence mechanisms in $CaSO_4$:Dy

1990 J. Phys.: Condens. Matter 2 1619

(http://iopscience.iop.org/0953-8984/2/6/020)

J. Phys.: Condens. Matter 2 (1990) 1619–1634. Printed in the UK

An electron spin resonance study of thermoluminescence mechanisms in $CaSO_4$: Dy

Mark D Morgan† and Thomas G Stoebe
Department of Materials Science and Engineering, University of Washington, FB-10, Seattle, WA 98195, USA

Received 5 September 1989

Abstract. Mechanisms of thermoluminescence (TL) in $CaSO_4$: Dy are studied using electron spin resonance (ESR) in single-crystal samples. The ESR analysis indicates the presence of several variations of a distorted SO_4^- centre locally stabilised by a nearest neighbour Ca vacancy. This centre's structure, which has not been reported previously, relates to several centres observed in this system and could also explain results in related compounds. The presence of the Dy impurity, which increases the concentration of Ca vacancies due to charge neutrality requirements, enhances both the concentration of these centres and the intensity of the major TL peaks near 220 and 350 °C. The specific role of these and other previously reported centres in the TL of this material is followed using heat treatments. This enables one to identify centres that change in the range of the observed TL peaks as well as centres that seem to be related to one another by charge transfer or rearrangement. The behaviour of the observed centres and their relationship to the TL behaviour of the system reemphasises the complexity of this system.

1. Introduction

Calcium sulphate doped with rare earth impurities is a sensitive thermoluminescent radiation dosemeter material with applications in personnel dosimetry and environmental monitoring [1, 2]. In spite of its widespread use, the mechanisms responsible for the thermoluminescence (TL) in this material are not well understood. This is due to several factors, including the difficulty of obtaining single crystals for study and the complex nature of this system [3, 4]. Most studies in $CaSO_4$ have utilised powder samples and/or natural single crystals of the $CaSO_4$ mineral (anhydrite). Unfortunately, these samples have contained a large number of crystal lattice defects, both intrinsic and extrinsic, several of which influence the TL in these materials [5, 6]. To aid in understanding effects due to impurities and other defects, Danby *et al* performed experiments on pure laboratory grown $CaSO_4$ single crystals [7–9]. The present work takes the next logical step by studying the defects present in laboratory grown doped single crystals of $CaSO_4$: Dy and the influence of these defects on the TL behaviour of this material.

This research utilised electron spin resonance (ESR) as the primary mode of identifying the defects present in this material. In this paper, several of the more prominent ESR centres observed at liquid nitrogen temperatures in gamma-irradiated $CaSO_4$: Dy

† Current address: Boeing Aerospace and Electronics, PO Box 24969, Mail Stop 9E-94, Seattle, WA 98124-6269, USA.

0953-8984/90/061619 + 16 $03.50

are reported and discussed. These and other centres reported in the literature are then followed through a TL read-out cycle and are related to the glow curve structure of this material. Utilising earlier work of the authors [10] along with related optical absorption work published elsewhere [11], these results allow the development of a more extensive understanding of the TL process in this material.

2. Crystallography and point defects

To understand the ESR centre models used in this work, an understanding of the crystal structure of $CaSO_4$ is vital. The calcium coordinated substructure of orthorhombic β-$CaSO_4$ structure, consisting of six SO_4 groups surrounding each Ca^{2+} ion, is illustrated in figure 1. The corners of the twelve-sided polyhedron in the centre represents the eight oxygens that surround each calcium atom. In this structure, there are symmetry-related oxygen ions that are important aids in modelling the ESR centres. Figure 2 shows the basic CaO_8 polyhedron with labels for the oxygen ions for future reference.

Due to the orthorhombic symmetry, this structure contains four pairs of equivalent oxygens. According to the nomenclature in figure 2, these are: O_G–O_H, O_A–O_B, O_E–O_F

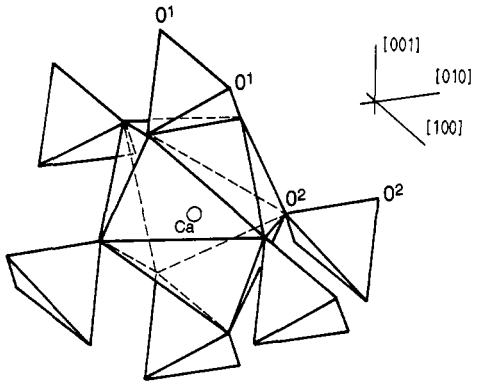

Figure 1. View of the Ca–6(SO_4) coordination substructure of β-$CaSO_4$. O^1 indicates oxygen ions aligned along [100] while O^2 indicates oxygen ions aligned along [010].

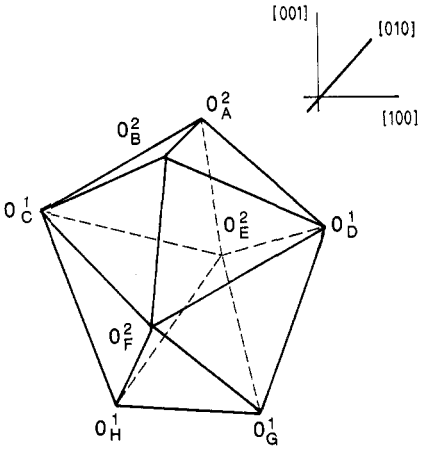

Figure 2. Schematic representation of the CaO_8 dodecahedron substructure with oxygen ions labelled. Structurally equivalent oxygen sites are A–B, C–D, E–F and G–H.

and O_D–O_C. In addition to these designations, the oxygen pairs in this structure can be classified according to the crystal axes in which they reside: O^1-type oxygen pairs are found along the [100] direction and O^2-type pairs are along the [010] crystal direction. This nomenclature is similar to that utilised by Bershov *et al* [12].

Doped $CaSO_4$ crystals can contain non-equilibrium concentrations of vacant lattice sites due to the requirements of charge neutrality. Dy^{3+} ion doping causes the formation of Ca^{2+} vacancies (denoted V_{Ca}) unless a monovalent ion such as Na^+ is present, in which case the Na^+ can compensate for the Dy^{3+} depending on their relative concentrations. The Dy^{3+} and Na^+ dopants are used in this study to determine the influence of V_{Ca} on the ESR spectrum and on the TL behaviour of the system; high Dy and low Na create high V_{Ca} concentrations while high Na concentrations decrease this vacancy concentration.

3. Experimental procedure

The crystal growth method used was based on the method first reported by Yamashita *et al* [13], with modifications to provide better control and large (up to 5 mm) monocrystals [11]. X-ray diffraction studies of the $CaSO_4$:Dy samples grown from acid solution all demonstrated the β-$CaSO_4$ anhydrite structure. Orientation of the crystals was accomplished by analysis of Laue back-reflection x-ray patterns. The dopants Dy and Na were added to the starting materials as Dy_2O_3 and as Na_2SO_4; concentrations reported were determined using inductively coupled plasma spectroscopy analysis.

All samples were subject to heat treatments at 500 °C for 24 hours after growth but prior to testing. The samples were placed in alumina boats, then surrounded by powdered $CaSO_4$ to reduce thermal shock and heated in an inert helium atmosphere furnace. After the heat treatment, the samples were quenched to room temperature by removing them from the furnace and placing them on an aluminium block. Samples to be irradiated were then exposed to a 30 000 Ci ^{60}Co source at an exposure of 1×10^6 R.

Step heat treatments were performed subsequently in conjunction with the ESR experiments to follow the evolution of the various ESR centres. These were carried out in air in a tube furnace controlled manually, in the TLD reader or in the ESR cavity. Each treatment consisted of heating times ranging from 1 to 7 min, after which the sample was removed and allowed to air cool (from the furnace) or was cooled *in situ* (in the TL reader). In the case of the ESR cavity, the samples were cooled relatively rapidly, directly from the heat treatment temperature to liquid nitrogen temperature.

The ESR spectrometer used in this work was a Varian model E-3 operating at microwave frequencies ranging from 8.8 to 9.5 GHz. Liquid nitrogen temperature measurements used a specially designed finger dewar which fit into the sample cavity. To suspend the samples in the dewar, a Teflon crystal holder was attached to the end of a quartz rod. This quartz rod fitted into a goniometer which allowed the sample to be rotated about the z axis of the cavity. DPPH and proton resonance was used to measure the magnetic field to within 0.02 G.

The TL measurements were performed in this study using a Harshaw Thermoluminescence Dosimeter (TLD) reader model 2000A coupled with a Harshaw model 2080 TL analyser. The heating rate used was programmed at 1 °C s^{-1}. All TL samples were ground to powder to ensure good thermal conduction between the sample and heater. The typical TL readout for $CaSO_4$: Dy at this heating rate shows glow peaks near 80, 115, 220 and 350 °C [14].

4. Results and discussion

4.1. Electron spin resonance results

Electron spin resonance was utilised in this work to study the gamma-radiation induced defect centres formed in $CaSO_4$ doped with Dy and/or Na. Utilising the principle g-values and the orientational dependence of the single crystals, a model for each centre was proposed. Subsequent isochronal heat treatments were then used to monitor the intensity of the centres as a function of temperature.

A typical ESR spectrum of $CaSO_4$:Dy, observed immediately after irradiation, is shown for one orientation in figure 3. Below the spectrum is a stick diagram labelling important centres discussed in this paper and elsewhere [11, 15]. Figure 4 shows a typical ESR scan of $CaSO_4$:Dy after a step heat treatment to 180 °C, demonstrating the changes that take place in the spectrum upon heating. It should be noted that in scans of unirradiated samples, no ESR signals were detected to the limit of sensitivity of the equipment, and that all the ESR centres discussed were detectable principally at liquid nitrogen temperatures.

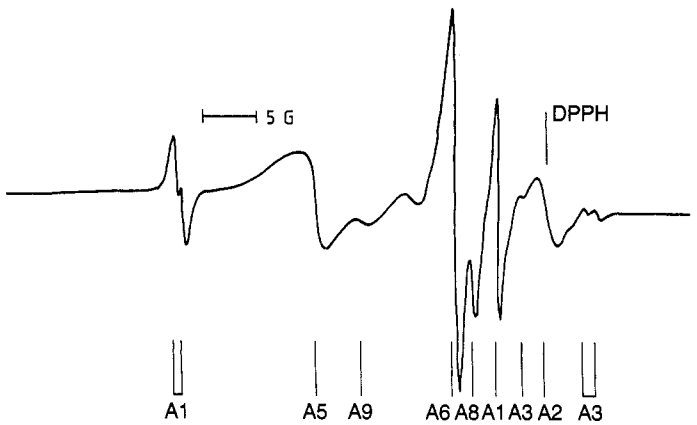

Figure 3. ESR spectrum of gamma-irradiated $CaSO_4$:Dy without prior heat treatment. Signals are identified according to the nomenclature in the text. This spectrum is observed at a crystal orientation in which the crystal has been rotated about the [001] axis to the point where the magnetic field is 60° from [100].

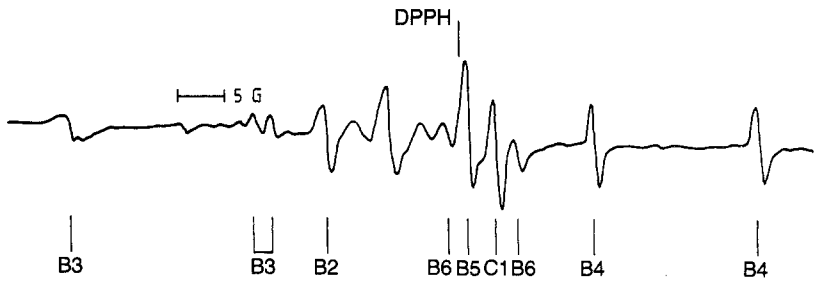

Figure 4. ESR spectrum of gamma-irradiated $CaSO_4$:Dy after heat treatment at 180 °C for 5 min in a tube furnace in air. Spectrum observed at same orientation as figure 3.

It is worthwhile first to make some general observations concerning these spectra. As can be seen from figures 3 and 4, all signals observed were within ±50 G of each other and were centred approximately on the free electron resonance line ($g = 2.0023$). With only one exception, observed g-values were found to be anisotropic, with the majority within ±0.03 of the free electron g-value. The linewidth of the signals, taken as the distance between the peaks of the ESR signal, were of the order of 0.5 to 2.5 G.

These observations are consistent with the idea that these signals are due to paramagnetic inorganic radicals trapped in the crystal structure of $CaSO_4$. In general, free radicals in crystals exhibit narrow linewidths due to their dilute concentrations, and, because of their symmetry and non-degenerate ground state, exhibit g-values comparable to that of the free electron [16].

Plots of the square of the g-value versus crystal orientation for each centre were utilised in the analysis of the observed ESR lines. One such plot, for centre A1, is shown in figure 5. The anisotropy seen in this type of data is evident in the splitting seen; in this case, the magnetic field was directed in one of the three mirror planes, so only two lines are observed. However, a random orientation yields four lines (three are seen in figure 3), while orientation of the magnetic field along one of the crystal axes causes the lines to coalesce, as also seen in figure 6.

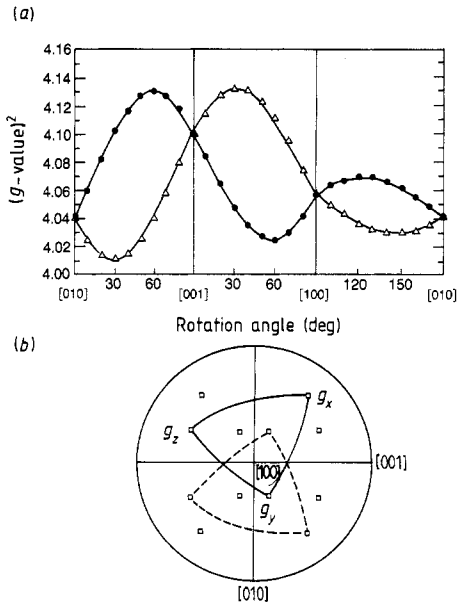

Figure 5. (*a*) Angular dependence of the square of the g-value, as explained in the text. (*b*) Stereographic projection of the magnetic axes of defect centre A1.

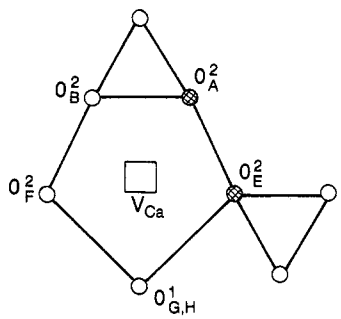

Figure 6. Structural model of the defect centre A1, viewed along [100].

The centres for which *g*-tensors were obtained in this study are discussed in three main groups according to their thermal stability:

(i) centres occurring in irradiated material prior to any heat treatments, labelled A1 to A10;

(ii) centres occurring in irradiated samples after heat treatment up to 200 °C, labelled B1 to B4;

(iii) centres occurring in irradiated samples after heat treatments at or above 200 °C, labelled C1 and C2.

Centres of the type B and C are referred to in this discussion as 'high temperature centres', while type A centres are referred to as 'low temperature centres'.

By applying ESR to irradiated $CaSO_4$:Dy, eighteen paramagnetic centres have been observed in this study [15]. It was possible to identify 13 of these centres as defects not directly linked to the impurity ions in the lattice, including five defects associated with Ca vacancies, five SO_3^- defects and three O_3^- defects. Three extrinsic paramagnetic centres were identified as associated with monovalent Na impurities [10]. The final two centres escaped identification.

4.1.1. Centre A1. The angular dependence of the *g*-values of centre A1 is shown in figure 5(*a*), with actual data points shown along with the best least squares fit curve for those points. The observed anisotropy demonstrates typical site splitting effects for an orthorhombic crystal symmetry. The angular behaviour of these lines is direct evidence for four structurally equivalent centres situated in magnetically inequivalent sites in the lattice which are related through symmetry operations.

The principle *g*-values obtained in this study are given in table 1 where they may be compared with related values from the literature. The average deviation from the free spin *g*-value is +0.0141, indicating that centre A1 is of the 'hole trap' variety. The direction cosines of the centre are shown in stereographic projection relative to the crystal axes in figure 5(*b*).

This centre was found to be thermally stable from room temperature to approximately 100 °C. The relative concentration of this centre, and consequently its ESR signal intensity, was found to be influenced by the dopant concentrations: an increase in intensity by about an order of magnitude was observed when going from undoped samples to samples doped with 0.1 mol% Dy. As the $CaSO_4$:Dy samples are doped with Na, the A1 centre intensity initially increases by a factor of 2 for a Na concentration of 0.1 mol%, then decreases by a factor of 3 for Na concentrations between 0.1 and 0.5 mol%.

This centre has been reported by Danby *et al* [7], who modelled it as an O^--type centre stabilised by a Ca^{2+} vacancy neighbour. However, Danby *et al* did not consider the change in symmetry that would be expected when a Ca vacancy is introduced as an oxygen nearest neighbour.

An analysis of the symmetry differences expected for an SO_4^- centre, with and without a Ca vacancy as a nearest neighbour to the SO_4 tetrahedron, leads to the expectation that the local symmetry of the sulphate tetrahedron itself would be altered to such an extent as to produce direction cosines that deviate from the crystal axes [15]. Further, with a loss of tetrahedral symmetry, one of the principle *g*-values is expected to be considerably greater than the free spin value and none of the other *g*-values are expected to be lower [17], as is observed. Using data available from this work and from other available sources, the present analysis suggests that the best structural model for

Table 1. Principal g-values and structural models of SO_4-type defect centres in sulphate lattices.

Material	g-values	Average	Structure	Reference
K_2SO_4	2.0037 2.0082 2.0486	2.0202	SO_4^-	[17, 18]
$K_2S_2SO_8$	2.0035 2.0084 2.0327	2.0150	SO_4^-	[19]
$BaSO_4$	2.0038 2.0066 2.0323	2.0142	V_{Ba}–SO_4^-	[20]
$CaSO_4$	2.0006 2.0091 2.0395	2.0164	V_{Ca}–O^-	[7]
$CaSO_4$: Y	2.0026 2.0078 2.0312	2.0139	O_2^{3-}–Y^{3+}	[12] (77 K)
$CaSO_4$: Y	2.0029 2.0122 2.0262	2.0138	O_2^{3-}–Y^{3+}	[12] (290 K)
$CaSO_4$: Dy	2.0022 2.0081 2.0386	2.0164	V_{Ca}–SO_4^-	This study (centre A1)

the A1 centre is actually a distorted SO_4^- centre locally stabilised by a (nearest neighbour) Ca vacancy.

This hypothesis may be further strengthened by comparing these results with other studies of SO_4^- centres. As can be seen in table 1, there is a remarkable equivalence among values obtained by various researchers in different sulphate lattices, even though some did not model these as SO_4^- type centres. Further, this model is also consistent, for the most part, with dopant dependence studies carried out in this work [15]. It was observed that Dy^{3+} dopant increased the A1 centre concentration by an order of magnitude; this is reasonable since Dy is expected to increase the concentration of Ca vacancies. As Na impurity is added, the A1 intensity initially increases, probably due to compensation of the charges of other impurities. After the concentration of Na increases to values greater than that of Dy, the Na causes a decrease in the Ca vacancy content which, in turn, destabilises A1 and decreases its population.

As the measurement temperature for centre A1 increases from 77 K towards room temperature, small changes in g-value are seen along with signal broadening. These changes, which are also present in the data of Danby *et al* [7–9] and in the related work of Bershov [12], lead to an expanded model for centre A1, which features two SO_4 tetrahedra interacting with the trapped hole, this structure being stabilised by a local Ca vacancy. At low temperatures the captured hole is localised at the sulphate tetrahedron which is closest to the stabilising vacancy and only a small amount of transfer to its neighbouring SO_4 complex is expected. In this centre, only the two sulphate ions

connected by O_B–O_F or O_A–O_E (figure 2) are considered due to stability considerations and interatomic distances. At higher temperatures, there is an increasing frequency of transfer between the two ions which would be expected to manifest itself through the centre observed by Bershov at 290 K; i.e., a hole trapped between the two oxygens of two adjacent sulphate ions which are locally compensated [12]. One would expect, adopting this expanded model, that the trace of this centre's g-tensor should remain constant since there is only a transfer of a hole between SO_4 ions without a substantial change in their electronic structure. This constant trace, in fact, was observed by Bershov [12].

Based on the above, it is proposed that the centre A1 must consist of a $(SO_4$–$SO_4)^{3-}$ centre, stabilised by local compensation in the form of a Ca vacancy, which has trapped a single hole. At high temperatures (>200 K) the hole is equally shared between sulphate sites, but at lower temperatures, the hole is trapped at the sulphate site containing an O_E or O_F oxygen since this ion is nearest the Ca vacancy. The connecting oxygen atoms are specific to the structure, being O_A–O_E or O_B–O_F. A schematic view of this centre is shown in figure 6.

4.1.2. Centre B1. Centre B1 was observed at heat treatment temperatures greater than about 150 °C, reaching a maximum intensity near 300 °C and then decaying to approximately 10% of this maximum value at 400 °C. While the B1 signal was detectable only at liquid nitrogen temperatures, a slightly different configuration of B1 was observed at room temperature in parallel to the modification to centre A1 seen at room temperature. The B1 defect centre was observed in $CaSO_4$:Dy samples and in $CaSO_4$:Dy containing low concentrations of Na; as the sodium concentration increased, the ESR signal intensity of B1 dropped rapidly below detectability.

The angular dependence of the g-value of centre B1 and stereographic projections of its direction cosines are shown in figure 7. The observed average g-value of B1 is 2.0109, also in the hole resonance centre classification.

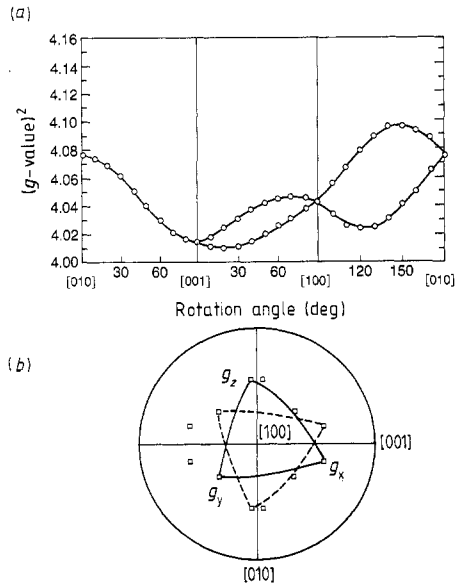

Figure 7. (*a*) Angular dependence of the square of the g-value. (*b*) Stereographic projection of the magnetic axes of defect centre B1.

An analysis of the properties of this centre and comparisons with work by Danby *et al* [7–9] and Bershov *et al* [12] indicates that B1 and the previously discussed A1 centres have much in common, and may be different configurations of the same defect. A1 and B1 have similar principle g-values as well as similar thermal properties. In addition, as A1 is decaying at $\simeq$100 °C, B1 is growing in intensity at about the same temperature.

The proposed model of the B1 centre, based on the present data, is similar to that for A1 except that it involves a different pair of SO_4 tetrahedra. The B1 configuration is the more stable of the two, leading to the expectation that the two SO_4 tetrahedra involved in B1 should be in closer proximity to each other than those of the A1 centre. In addition, by comparing the data for the room temperature form of B1 with Bershov's room temperature results [12], there is an indication that a hole is being shared between the O_H–O_C or O_G–O_D oxygen pairs. The best fit to the available data is a centre composed of two sulphate tetrahedra, stabilised by an adjacent Ca vacancy, sharing a trapped hole. The two adjacent oxygens in this case are the O_H–O_C or O_G–O_D pairs. At liquid nitrogen temperatures, the hole is localised at the SO_4 structure that contains an O_C or O_D oxygen since this would cause the least perturbation, being the closest oxygen to the vacancy. As the temperature is increased there is a higher probability for the hole to be transferred to the other SO_4. This would explain the signal broadening that Danby reported at temperatures above 215 K, as well as the presence of the modified B1 signal at room temperature. Adopting this model, one would expect that the trace of this centre's g-tensor should remain constant since there is only transfer of a hole between SO_4 ions without a substantially change in their electronic structure. This constant trace was observed in the present study. A schematic diagram of this centre is shown in figure 8.

4.1.3. Centres B2 and B3. The g-value angular dependence of centres B2 and B3 is shown in figure 9. The average g-values for B2 and B3 were found to be 2.0142 and 2.0154, respectively; the related centre B4 had an average g-value of 1.9958. These g-values suggest that B2 and B3 are hole traps, while B4 is an electron trap. The site splitting data of these centres predict that each centre is associated with four magnetically inequivalent lattice sites.

The correspondence between the principal g-values, the g-value angular dependence and the direction cosines of centres B2 and B3 indicate that they represent the same defect located in two different niches in the crystal lattice. Observed parallels between B3 and B4 suggest that these are the same centre, with B3 acting as a hole trap and B4 acting as an electron trapping centre. The ESR signals of centres B2 and B3 begin to grow at $\simeq$160 °C, with B2 being the centre with the greatest signal intensity, about 3.5 times larger than B3. B2 reaches an ESR intensity maximum at $\simeq$300 °C and B3 reaches a

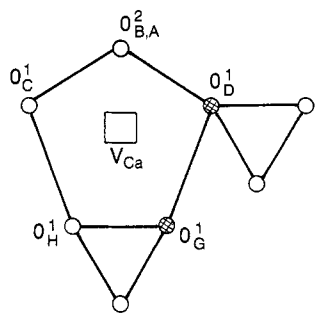

Figure 8. Structural model of centre B1, viewed along [010].

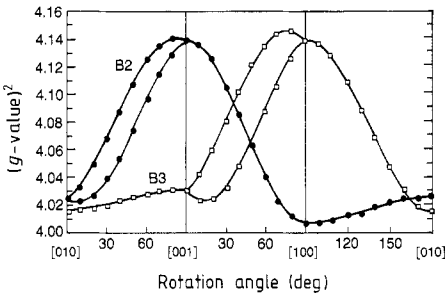

Figure 9. Angular dependence of the square of the g-values of centres B2 and B3.

maximum at a temperature of ≃250 °C. B3 is not detectable after three-minute heat treatment at 400 °C; while B2 remains detectable at 400 °C for up to five minutes. After one hour at 400 °C, B2 is no longer observed. This indicates that centre B2 has a greater thermal stability than that of centre B3. None of these centres were detectable in undoped $CaSO_4$ samples and it was observed that Na impurities in $CaSO_4$: Dy reduced their ESR signal intensities.

On analysing the stereographic projections of these centres, very good agreement was found between the principal values of B2, B3 and B4 and the $Ca\text{–}O^2_{E\,or\,F}$ and $Ca\text{–}O^1_{C\,or\,D}$ interatomic directions of the $CaSO_4$ structure. Centre B2 has its central Δg-value in the $Ca\text{–}O_{E\,or\,F}$ direction, while centres B3 and B4 have their maximum Δg-values when the magnetic field is in the $Ca\text{–}O_{C\,or\,D}$ direction. The principal g-values of centre B2 and of B3–B4 have direction cosines corresponding to the direction of the $O^1\text{–}O^1$ and $O^2\text{–}O^2$ bonds, respectively.

The average g-values for these centres match closely to those expected for SO_4^--type defect centres in a distorted sulphate lattice, as seen in table 1. These values reflect the deviation from the isotropic g-tensor of the free SO_4^- ion [16]. The largest deviation from the free electron g-value is expected to occur in the direction of maximum distortion of the sulphate complex [16, 20]. In the normal $CaSO_4$ lattice this would occur in the [001] direction [21]. However, SO_4^- radicals are not stable in the sulphate lattice if they are not trapped at virtual negative sites [7, 20], i.e. at a local Ca vacancy in $CaSO_4$. Since there are several different possible positions for the Ca vacancy with respect to the sulphate ion, it is likely that a position leading to the smallest perturbation would be preferred. If this is correct, there are two pairs of sites, the pairs being related by mirror planes, which are associated with the $O_{C\,or\,D}$ and $O_{E\,or\,F}$ oxygens in the structure.

The proposed structure of B3 is that of an SO_4^- ion with a Ca vacancy adjacent to an O^1 oxygen. This would result in distortion around the $O^1\text{–Ca}$ direction leading to the largest principal g-value in that direction. B2 is associated with the $Ca\text{–}O^2$ direction, which would indicate an SO_4^- ion with a Ca vacancy adjacent to an O^2 oxygen. In both of these models, the trapped hole is predominantly localised on the O^1 or O^2 oxygen adjacent to the vacancy. Schematic diagrams of centres B2 and B3 are shown in figure 10.

4.1.4. Centre C1. This centre is first observed after a 200 °C heat treatment and decays after approximately one hour at 400 °C. This is an almost axial centre with average g-value of 1.9821, which indicates that it is an electron trap. The direction of the g-values are along the crystal axes with the maximum deviation from the free electron g-value occurring along the [010] direction ($g_x = 1.9415$). No site splitting of the signal was observed for any orientation. Centre C1 was detected in $CaSO_4$: Dy samples and at low

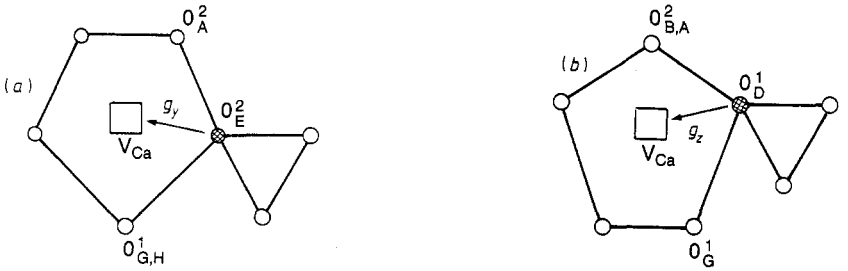

Figure 10. Structural models of: (*a*) centre B2, viewed along [100]; (*b*) centre B3, viewed along [010].

intensities in undoped samples. Low concentrations of Na in $CaSO_4$: Dy did not change the ESR intensity of this centre; however, the C1 signal level did decrease with increasing Na content.

It is difficult to assign a structural model to this centre due to the lack of additional data, including hyperfine information. The extreme thermal stability of this centre along with the direction cosine information may indicate a single atom defect—most likely, from *g*-value comparisons, an oxygen ion O^-. However, no hyperfine interaction was identified and without more information further speculation at this point is not useful.

4.1.5. Centre C2. Centre C2 is the only isotropic centre observed in this study. With a *g*-value of 2.0027, this centre is very near the free electron value. The linewidth of this centre is $\simeq$7.1 G and is the broadest signal that was observed in this material.

At low concentrations of Na ($\simeq$0.1 to 0.5 mol%), this signal was detected in irradiated samples after heat treatment at 450 °C. It was also observed, at reduced intensity, after a 24 hour, 450 °C anneal in inert atmosphere. This centre was not detected in undoped $CaSO_4$ or in $CaSO_4$: Dy.

The wide linewidth and occurrence only after high temperature treatments may indicate a single impurity defect in a number of different crystal sites or orientations. However, without additional information, it is difficult to assign a meaningful model to this defect.

4.1.6. Other paramagnetic centres. A variety of paramagnetic centres observed and identified in other studies were also seen in this work. Sulphur–oxygen radicals such as SO_3^- and O_3^- have been observed in numerous sulphate lattices [7–9, 12, 17–20]. In this study, the SO_3^- centres, designated A2–4, occupy three different lattice sites in the $CaSO_4$ structure, two different orientations within the SO_4 site and one interstitial site. High temperature forms of these SO_3^- centres were also observed at $\simeq$280 °C. Four O_3^- centres, called A5–8, were observed in this material, with each O_3^- in a different lattice site. These findings compared well with Bershov *et al* [12]. Centres A9 and A10 compare well with the O_2^{3-}–Na^- centre of Bershov *et al* [22].

4.2. Step heat treatment results

Step heating using the Harshaw 2080 TL reader was used to get a realistic picture of which centres appeared, which centres changed, and at what temperatures, during the TL readout cycle. These results are presented in figure 11. Here, the sample was heated

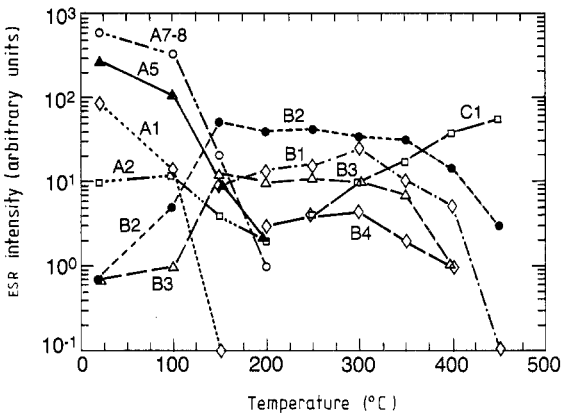

Figure 11. Thermal decay of ESR centres in $CaSO_4$: Dy using the Harshaw 2080 TL reader as a step heater. Centres are labelled according to the nomenclature in the text.

progressively for one minute at each temperature indicated, cooled to room temperature *in situ*, then cooled to liquid nitrogen temperature for ESR read-out. Other step heat treatment experiments showed similar relationships between centres, except that longer heating times reduced the temperature at which the respective peaks decayed.

By comparing the glow curve structure with the step heat treatment decay data seen in figure 11 and in other experiments, correlations may be made between glow peak temperatures and the decay temperatures of observed centres. In the region of TL peak 1 (70–90 °C) and peak 2 (100–130 °C), all of the 'A' peaks decay, but at different rates. Some of the centres seem to decay in two stages, partly in the range of peak 1, then fully in the range of peak 2, although the results of different types of experiment were not always consistent. Centres that show major decay in the thermal region of TL peak 1 include A1–6, A9 and A10. In the TL peak 2 region, ESR centres A1, A2, A5, A7 and A8 are observed to decay. It should be noted that A1 decays initially by about one order of magnitude in the region of peak 1, then to a non-detectability in the range of peak 2.

It is somewhat difficult to correlate the ESR centres with the higher temperature TL peaks because of expected charge redistribution that can occur during the step heat treatment experiment. Retrapping and other redistribution of charge can occur during the cooling of the sample to room temperature, which required several seconds in most of our heat treatment experiments, as well as while the sample is at room temperature and during further cooling to liquid nitrogen temperature. This affects especially our ability to correlate directly peak temperatures to ESR peak changes in the higher temperature regions. However, general correlations indicate that the 'growing-in' of centres B1, B4 and perhaps B2 and B3 are the events that are most likely to be involved with TL peak 3 (150–260 °C), while the decay of the B centres above 300 °C may also be associated with the 300–350 °C peak.

The heat treatment in the ESR cavity was an especially useful experiment since it allowed a rapid cool directly to 77 K, minimising charge redistribution during the cooling process. The effects of this more rapid cool were directly observable, as noted below. The maximum temperature that could be achieved with the ESR cavity heater was 180 °C. It was expected, from reviewing figure 11, that the high temperature centres would begin growing in at temperatures below 180 °C after annealing in the ESR cavity. This was not observed. While centre B1 did begin to appear at 170 °C, this experiment did not produce

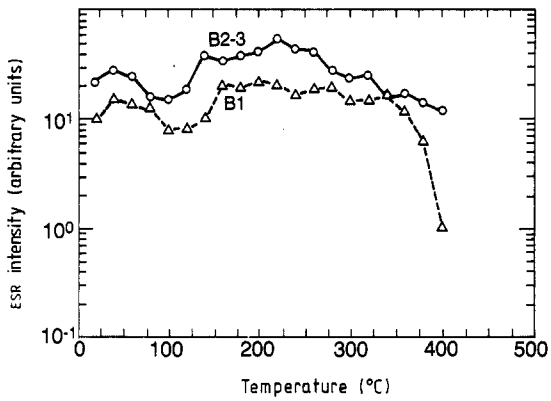

Figure 12. ESR intensity of centres B1, B2 and B3, observed after step heat treatment of irradiated $CaSO_4$: Dy. Prior to this experiment, these samples had been heat treated at 180 °C and stored 9 h at room temperature.

either B2 or B3 centres. This indicates that the observation of these peaks after heat treatment at this temperature in the other experiments is a result of charge redistribution during the slower cooling processes in those other experiments.

After this 180 °C heat treatment in the ESR cavity and the subsequent ESR measurement, the crystal was stored at room temperature for nine hours and then a subsequent ESR scan was taken. This latter revealed that all of the high temperature centres had become repopulated during the nine-hour room temperature storage. Figure 12 shows the succeeding step anneal of this sample for centres B1, B2 and B3, done in the annealing furnace, starting at room temperature and proceeding to 400 °C. These high temperature centres demonstrate a slight decrease in intensity at the temperatures that were observed above to cause decay of the low temperature centres; they subsequently decay at temperatures close to those observed in figure 11.

These results are taken as evidence that the high temperature centres are present at room temperature after irradiation, but are not normally ESR-active. The long storage time apparently allows the rearrangement of charge among the various traps during the room temperature storage, allowing the ESR signals from these centres to be observed.

Based on these observations, the traps associated with Ca vacancies (B1, B2 and B3) are assigned as two hole traps. That is, during irradiation these Ca vacancies, which are virtual -2 charge sites in the lattice, trap two holes. Since the two holes are paired at this site, this centre will not be visible with ESR. During heating, the first hole will be released at a certain temperature, leaving an unpaired electron in the centre and making it visible with ESR at that temperature. The centre will appear to 'grow-in' at this temperature and TL can be produced by the release of this first hole. The observation that the B1 centres 'grow-in' at about the same temperature at which the A1 centres are decaying indicates that both centres lose a hole in the same temperature range. This is expected since the natures of the two centres are so similar.

In the room temperature storage experiment, the B centres after storage are populated with just one hole due to charge rearrangement, rendering them visible as B centres in ESR. As the temperature continues to rise, the remaining hole is eventually released, resulting in the decay of the ESR signal of that centre and another TL peak.

The decrease in signal of the high temperature centres at the annealing temperature of the A centres, as seen for centres B2 and B3 in figure 12, may be related to a retrapping

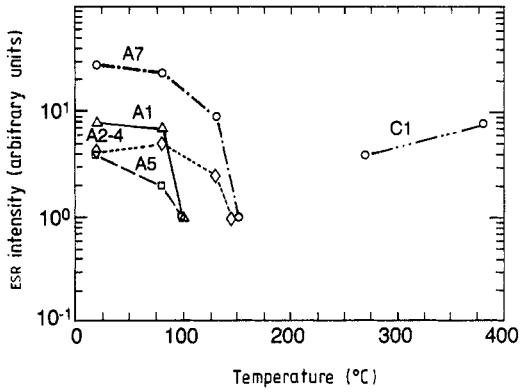

Figure 13. ESR intensity of observed centres after step heat treatment of undoped $CaSO_4$.

of holes released by the A centres at this temperature by the B centres. Evidence of retrapping by some of the low temperature traps was also observed. This information would imply that the $CaSO_4$ system has a large number of traps, both paramagnetic and non-paramagnetic, which come into play during a TL readout cycle.

Step heat treatment experiments were also performed on undoped samples of $CaSO_4$ to further determine the relationship between the observed trapping centres and TL behaviour. These samples showed glow peaks near 80 and 120 °C with a smaller peak centred at 175 °C. The heat treatment results from this experiment are shown in figure 13. Notice the lack of B centres when dopants are absent, which accompanies the lack of glow peaks at high temperatures. This confirms that the Dy dopant is vital in either the creation or stabilisation (or both) of high temperature traps, and that the high temperature defect centres are important in the development of the high temperature TL peaks in $CaSO_4$.

5. Models for TL behaviour

The ultimate goal of this investigation is to seek a quantitative understanding of the behaviour of the defect processes that govern the TL mechanisms, and to control or modify these processes in desirable ways. Models provide the first step with which complex phenomena can be understood.

Based on the results presented above and elsewhere [11, 15], it is proposed that TL peak 1 near 80 °C is a result of the decay of the following lattice defect centres: SO_3^- (A2–4), O_3SO_A–V_{Ca}–O_ESO_3 (A1), and O_3^-–Na^+ (A9–10). Peak 1 may also include partial decay of O_3^--centres A5 and A6. It is likely that the defects associated with the monovalent sodium ion and the Ca vacancy centre are the major trapping species because of the positive effect of Na and heat treatments, both of which can affect changes in Ca vacancy concentration, on the intensity of glow peak 1.

Peak 2 near 120 °C appears to correlate best with the decay of the ozonide group of defect centres, observed as ESR centres A5, A7 and A8. These O_3^- defects occupy three different sites in the $CaSO_4$ lattice; they are hole trap centres which release their charge near 120 °C. Further decay of ESR peaks A1 and A2 is also seen in this region; however, the role of these centres in peak 2 must be minor, since peak 2 is less sensitive to V_{Ca} content than peak 1 [15].

Peak 3 occurs in the temperature range 150 °C to 260 °C and is due to holes being released from Ca vacancy two-hole trap centres. There are four such two-hole trap centres (ESR centres B1–4) which release their first trapped hole in the vicinity of 200 °C: O_3SO_H–V_{Ca}–O_CSO_3, V_{Ca}–$(O_ESO_3)^-$, V_{Ca}–$(O_DSO_3)^-$, and V_{Ca}–$(O_SSO_3)^-$. After irradiation, two holes are trapped at specific oxygens adjacent to the vacancy; these two holes form a pair and consequently are not observed with ESR. As the first hole escapes, the remaining hole will form a paramagnetic centre and will be observed with ESR. This is seen as a 'growing-in' of these vacancy centres near 200 °C and the release of TL in the form of peak 3. The second hole is liberated at temperatures near 350 °C. It should be noted that coupled traps of this type can contribute to the observed irradiation dose dependence of the glow peak temperature in $CaSO_4$, a point that may be relevant to models developed to explain such effects [4].

Peak 4, which has a low intensity and is often obscured by peak 3, corresponds to the temperature range 300 °C to 380 °C. The model for this peak relates to the second hole released from the V_{Ca} centres O_3SO_H–V_{Ca}–O_CSO_3 and V_{Ca}–$(O_DSO_3)^-$, and the decay of SO_3^- centres.

Another trapping centre, C1, begins to 'grow-in' near 300 °C. This is proposed to be an O^- electron centre. This centre decays at $\simeq$500 °C and should be related to the trapping centre for peak 5, which occurs near 530 °C.

The observation of TL peaks 3 and 4 depends on the presence of the Dy dopant in the $CaSO_4$ lattice. Dy is a trivalent cation which will enhance the Ca vacancy concentration due to charge balance in the crystal, thus enhancing the content of sulphate–Ca-vacancy defect complexes. In addition, the presence of Dy may provide additional stability for the B centres, since TL from these centres is not seen in undoped samples.

The identity of the recombination centre has not been determined in this study; however, it is known from previous work that the recombination centre(s) emit energy near the wavelength of 335 nm [23]. It has also been shown that the energy of recombination is transferred to the Dy ion that emits the TL [10, 11].

Acknowledgments

The authors wish to thank Professor A Kwiram for his assistance in providing access to the ESR equipment and in interpreting some of the results. One author (MDM) was partially supported in this work by training grant CA09081-05 from the US Department of Health and Human Services. Portions of this research were supported by Teledyne Isotopes, Inc.

References

[1] Horowitz Y S 1984 *Thermoluminescence and Thermoluminescent Dosimetry* vol 1, ed Y S Horowitz (Boca Raton, FL: CRC) pp 89–172
[2] Becker K 1973 *Solid State Dosimetry* (Boca Raton, FL: CRC)
[3] Lakshmanan A R, Chandra B and Bhatt R C 1978 *Nucl. Instrum. Methods* **153** 581–8
[4] Srivastava J K and Supe S J 1983 *J. Phys. D: Appl. Phys.* **16** 1813–8
[5] Nambi K S V, Bapat V N and Ganguly A K 1974 *J. Phys. C: Solid State Phys.* **7** 4403–15
[6] Matthews R J and Stoebe T G 1982 *J. Phys. C: Solid State Phys.* **15** 6271–80
[7] Danby R J, Boas J F, Calvert R L and Pilbrow J R 1982 *J. Phys. C: Solid State Phys.* **15** 2483–93
[8] Danby R J 1983 *J. Phys. C: Solid State Phys.* **16** 3673–8
[9] Calvert R L and Danby R J 1984 *Radiat. Protect. Dosim.* **6** 55–7

[10] Morgan M D and Stoebe T G 1986 *Radiat. Protect. Dosim.* **17** 455–8
[11] Morgan M D and Stoebe T G 1989 *J. Phys.: Condens. Matter* **1** 5773–81
[12] Bershov L V, Martirosyan V O, Marfunin A S and Speranskii A V 1971 *Phys. Status Solidi* b **44** 505–12
[13] Yamashita T, Nada N, Onishi H and Kitamura S 1968 *Proc. 2nd Int. Conf. Luminescence Dosimetry (Gatlinberg, TN)* (Oak Ridge National Laboratory CONF-680920) pp 4–17
[14] Stoebe T G and Morgan M D 1984 *Thermoluminescence and Thermoluminescent Dosimetry* vol 1, ed Y S Horowitz (Boca Raton, FL: CRC) pp 19–47
[15] Morgan M D 1986 *PhD Thesis* University of Washington, Seattle (available from University Microfilms, Ann Arbor, MI)
[16] Atkins P W and Symons M C 1967 *The Structure of Inorganic Radicals* (New York: Elsevier)
[17] Gromov V V and Morton J R 1966 *Can. J. Chem.* **44** 527–8
[18] Morton J R 1967 *J. Phys. Chem.* **71** 89–92
[19] Atkins P W, Symons M C R and Wardale HW 1964 *J. Chem. Soc. Faraday Trans.* I 5217
[20] Krystek M 1980 *Phys. Status Solidi* a **57** 171–8
[21] Kirfel A and Will G 1980 *Acta Crystallogr.* B **36** 2881–90
[22] Bershov L V, Martirosyan V O, Marfunin A S and Speranskii A V 1975 *Fortschr. Miner.* **52** 591–604
[23] Tomita A and Tsautsumi T 1978 *Japan. J. Appl. Phys.* **17** 453–4